Journal of Inorganic Biochemistry 194 (2019) 200–213

Contents lists available at ScienceDirect

Journal of Inorganic Biochemistry

journal homepage: www.elsevier.com/locate/jinorgbio

Modulating the antitumoral activity by the design of new platinum(II) compounds: Synthesis, characterization, DFT, ultrastructure and mechanistic studies

Rafaela O. Moreira[a], Samila R. Morcelli[a], Milton M. Kanashiro[b], Jackson A.L.C. Resende[c,d], Leide L.F. Maciel[b,e], João Carlos de A. Almeida[e], Lawrence R. Gahan[f], Adolfo Horn Jr[a], Christiane Fernandes[a,*]

[a] Laboratório de Ciências Químicas, Universidade Estadual do Norte Fluminense Darcy Ribeiro, 28013-602 Campos dos Goytacazes, RJ, Brazil
[b] Laboratório de Biologia do Reconhecer, Universidade Estadual do Norte Fluminense Darcy Ribeiro, 28013-602 Campos dos Goytacazes, RJ, Brazil
[c] Laboratório de Difração de Raios X, Universidade Federal Fluminense, 24020-150 Niterói, RJ, Brazil
[d] Instituto de Ciências Exatas e da Terra, Campus Universitário do Araguaia, Universidade Federal do Mato Grosso, 78600-000 Barra do Garças, MT, Brazil
[e] Laboratório de Fisiologia e Bioquímica de Microorganismos, Universidade Estadual do Norte Fluminense Darcy Ribeiro, 28013-602 Campos dos Goytacazes, RJ, Brazil
[f] School of Chemistry and Molecular Biosciences, The University of Queensland, Brisbane, QLD 4072, Australia

A B S T R A C T

The synthesis, physico-chemical characterization, Density functional theory (DFT) calculation and cytotoxicity against five human tumoral cell lines (THP-1, U937, Molt-4, Colo205 and H460) of four new platinum(II) coordination compounds are reported, *i.e.* [Pt(HL1)Cl]·H_2O (**1**), [Pt(HL2)Cl]·H_2O (**2**), [Pt(HL3)Cl]·H_2O (**3**) and [Pt(HL4)Cl]·H_2O (**4**). The ligands contain N2O donor sets. Furthermore, H2L3 and H2L4 present α and β-naphthyl groups respectively, which are absent in HL1 and H2L2. X-ray diffraction studies were performed for complex (**3**), indicating the formation of a mononuclear platinum(II) complex. Complexes (**3**) and (**4**), which contain α and β-naphthyl groups respectively, have presented lower IC_{50} (inhibitory concentration) values than those exhibited by complexes (**1**) and (**2**). The mechanism of cell death promoted by complexes (**3**) and (**4**) was investigated, suggesting that, toward U937 cell line, the α isomer promotes death by apoptosis and the β isomer by necrosis. Transmission and scanning electron microscopy investigations are in agreement with the loss of mitochondrial membrane potential ($\Delta\Psi m$) observed by JC-1 mitochondrial potential sensor and indicate that the activity of complex (**3**) against U937 cell line is mediated by an apoptotic mechanism associated with mitochondrial dysfunction. A quantification of caspases 3, 6, 8 and 9 indicated that both the intrinsic and extrinsic pathways are involved in the apoptotic *stimuli*. Based on DFT calculations all the Pt(II) complexes present the same coordination environment for the metal centre, indicating that the higher cytotoxic activities exhibited by complexes (**3**) and (**4**) are related to the presence of the α and β-naphthyl groups in the ligand structure.

1. Introduction

The development of new platinum antitumor drugs has been motivated by the usefulness of cisplatin and derivatives in chemotherapy and the resistance of many tumors to these compounds [1]. The four main steps in the mechanism of action of cisplatin are: cellular uptake, aquation/activation, DNA platination and cellular processing of Pt-DNA lesions, leading to cell survival or apoptosis [2]. Numerous studies show that cisplatin forms in DNA ~90% intrastrand cross-links (CLs) between neighboring purine bases (1,2-GG or 1,2-AG intrastrand CLs) and remaining lesions are intrastrand CLs between purine bases separated by a third base, interstrand CLs and monofunctional adducts [3]. The interaction of cisplatin with DNA causes significant distortion of helical structure and results in inhibition of DNA replication and transcription, driving the cell to die by apoptosis [4]. Cisplatin is the first generation of platinum-based drugs (PBDs) used as anticancer agents, inducing dose-limiting toxicity on the cells. Due to the severe side effects (nephrotoxicity, ototoxicity, nausea and vomiting) and to overcome the resistance observed in some cancers, Carboplatin and Oxaliplatin were developed [5]. Recently, Gao and co-workers have reviewed the recent progress in research of platinum complexes as well as their biological activities and insights into the development and design of new platinum drugs [6].

In 2013, Souza and co-workers reported the high cytotoxicity in cisplatin resistant A2780cisR tumor cells (ovarian) as well as in breast cancer MCF-7, and reduced toxicity against LLC-PK1 cells (normal renal cells), of two novel platinum(II) complexes. These complexes, which present thiosemicarbazone in their structures exhibit high antiproliferative activity and very low nephrotoxicity, suggesting they are very specific on cancer cells. However, no mechanism of action was

* Corresponding author.
E-mail address: chris@pq.cnpq.br (C. Fernandes).

https://doi.org/10.1016/j.jinorgbio.2018.12.016
Received 16 June 2018; Received in revised form 22 December 2018; Accepted 24 December 2018
Available online 30 January 2019
0162-0134/

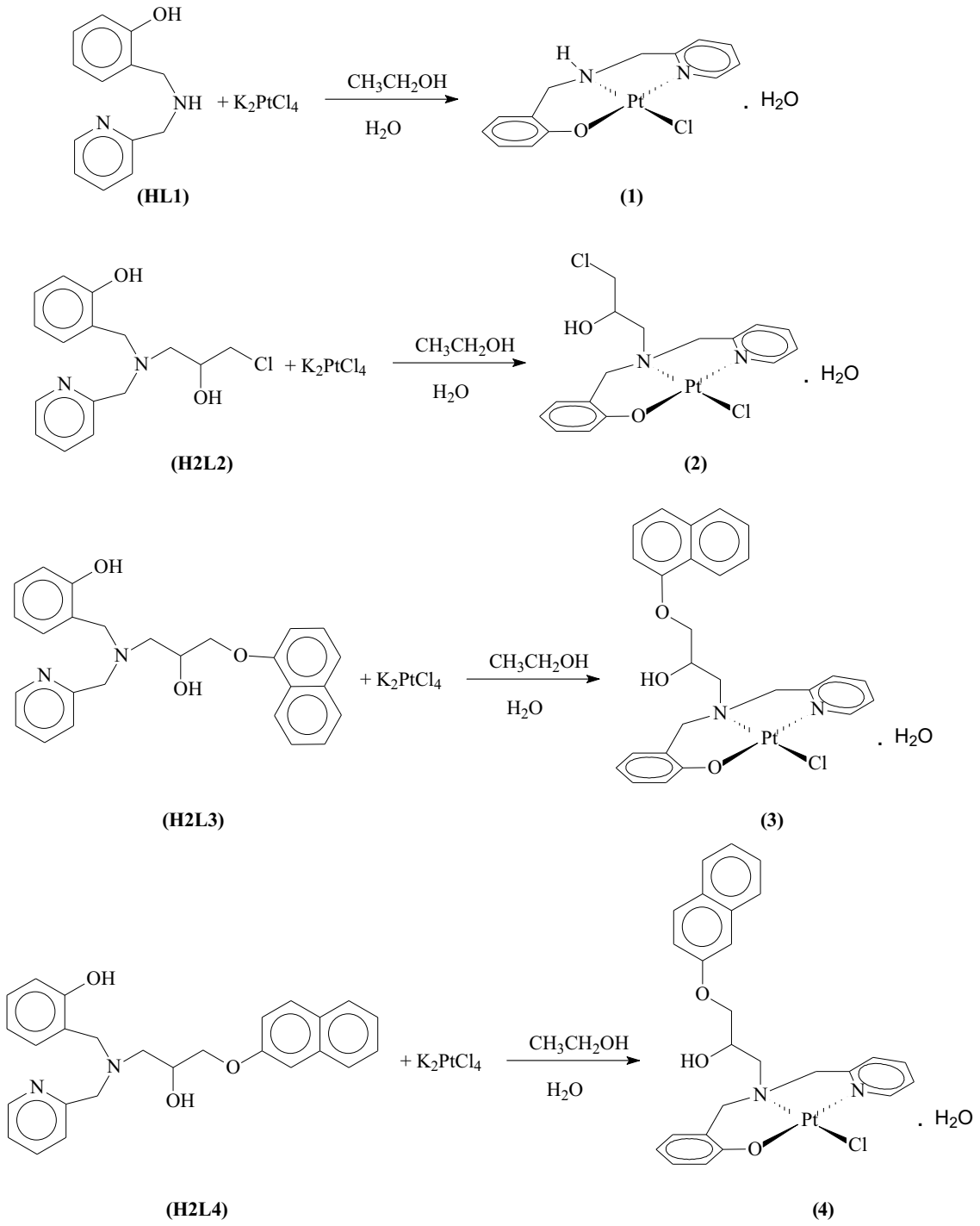

Scheme 1. Scheme illustrating the syntheses of the platinum(II) complexes (**1**)–(**4**).

proposed by the authors [7]. In 2016, Keppler and co-workers reported the investigation of cell ultrastructure and drug distribution in samples (murine tumor and kidney) obtained from mice treated with therapeutically relevant doses of two platinum(IV)-based anticancer compounds. These studies revealed cytoplasmic sulfur-rich organelles accumulating platinum in both kidney and malignant cells, showing high sensitivity [8]. Recently, Gou and co-workers have reported the cytotoxicity of new five platinum(IV) prodrugs conjugated with the potentiator Lonidamine (LND), which increases the response of human tumor cells to platinum(II) drugs in preclinical studies. LND works on the mitochondria, provoking disruption of the mitochondria transmembrane potential *via* a direct effect on the mitochondrial permeability transition pore (mPTP). The most cytotoxic complex triggered cancer cell death *via* an apoptotic pathway and effectively induced apoptosis in LNCaP cells, which is closely associated with mitochondrial function disruption and reactive oxygen species accumulation [9].

We have been investigating the coordination behavior of ligands HL1 and H2L2 (Scheme 1) with several transition metals, aiming to develop synthetic models for metalloenzymes and as metallodrugs. In 2015 we described the synthesis and antitoxoplasma activity of a Zn(II) complex, containing the ligand HL1 and sulfadiazine, the current medicine to treat the infection caused by *T. gondii* [10]. In 2016, we reported the synthesis, X-ray crystal structure and *in vitro* and *in vivo*

studies of the antineoplastic activity of the complex [Cu(HL1)Cl_2] against human keukemia THP-1 and murine melanoma B16-F10 cell lines. This complex presents LD_{50} (lethal dose) of 24 mg·kg^{-1} and showed a 92% inhibition of tumor growth in BALB/c nude bearing THP-1 tumor [11]. In 2018, we reported the antitumoral activity of a copper(II) complex [Cu(HBPA)(L1)Cl]3H_2O which was obtained through the reaction between the ligand stilbene-quinone (HL1) and the complex [Cu(HBPA)Cl_2]. Results from MTT assay [MTT = (3-(4,5-dimethyltiazol-2-yl)-2,5-diphenyl tetrazolium bromide)] revealed that this new complex is more active against sarcoma cell lines (MES-SA/Dx5 and MES-SA) than both the free ligand HL1 and complex [Cu(HL1)Cl_2], reducing cell viability to < 50 μM [12]. With regard to ligand H2L2, its coordination behavior has been studied with iron(III), copper(II), zinc(II) and nickel(II) ions [13–18]. In order to improve the biological activities presented by these coordination compounds, two new ligands H2L3 and H2L4, whose structures may be considered as derived from HL1 and H2L2 were developed. The attachment of naphthyl groups was successful and copper(II), cobalt(II) and iron(III) complexes were obtained and reported previously [19–21]. Copper(II) complexes were obtained as dinuclear in the solid state but form mononuclear species in solution [19]. The complex containing the ligand H2L3 (α isomer) exhibits higher activity than *cis*-platin against U937 and LD_{50} of 55 mg·kg^{-1}. Mechanistic investigations for this complex suggests that the apoptosis signal starts from an extrinsic pathway involving the activation of caspases 4 and 8. This signal is amplified by mitochondria with the concomitant release of cytochrome *a* and the activation of caspase 9 [19]. The synthesis, physico-chemical characterization and cytotoxicity toward five human tumoral cell lines (THP-1, U937, Molt-4, Colo205 and H460) of cobalt(II) complexes, obtained with the ligands H2L2, H2L3 and H2L4 were reported in 2016 [20]. Complexes containing the ligands H2L3 and H2L4 have presented IC_{50} values lower than those exhibited by complex containing the ligand H2L2. The complex containing the ligand H2L4 has presented IC_{50} values lower than *cis*-platin toward Colo205 and H460. Mechanistic investigation suggests that the cytotoxic activity of this complex against U937 cell line is mediated by an apoptotic pathway, associated with mitochondrial dysfunction [20]. Dinuclear iron(III) complexes, which presented moderate antitumoral activity, were obtained with ligands H2L3 and H2L4 [21]. Therefore, based on our results, we can state that the antitumoral activity of complexes containing the same ligands show dependence on the metal nature, nuclearity and the isomerism. In this sense, looking to develop new coordination compounds with increased antitumoral activity, we report herein the synthesis, characterization and antitumoral activity of four new platinum(II) complexes containing the ligands HL1, H2L2, H2L3 and H2L4: [Pt(HL1)Cl]H_2O (**1**), [Pt(HL2)Cl]H_2O (**2**) [Pt(HL3)Cl]H_2O (**3**) and [Pt(HL4)Cl]H_2O (**4**) (HL1: N-(2-hydroxybenzyl)-N-(2-pyridylmethyl)amine; H2L2: N-(2-hydroxybenzyl)-N-(2-pyridylmethyl)[(3-chloro)(2-hydroxy)]-propylamine; H2L3: 1-[2-hydroxybenzyl(2-pyridylmethyl)amino]-3-(1-naphthyloxy)-2-propanol and (H2L4): 1-[2-hydroxybenzyl (2-pyridylmethyl)amino]-3-(2-naphthyloxy)-2-propanol). The interaction with complex (**3**) with U937 cells was monitored *via* annexin staining, mitochondrial membrane potential (ΔΨm) analysis, cell cycle analysis, transmission electron microscopy (TEM), scanning electron microscopy (SEM) and quantification of caspases 3, 6, 8 and 9. Compared with the respective cobalt(III) complex previously reported by us [20], complex (**3**) is much more active confirming the relevance of the platinum on the biological activity.

2. Experimental

2.1. Materials and methods

The ligands and their respective platinum(II) complexes were synthesized using analytical grade reagents. UV–Vis, electrochemical and ESI(+)-MS investigations were carried out employing spectroscopic, HPLC or MS quality solvents. All chemicals and reagents were purchased from Aldrich and used as such. ^{1}H and ^{13}C NMR spectra were recorded with a JEOL eclipse 400+ spectrometer. Chemical shifts (δ) are given in ppm, and the spectra were recorded in appropriate, deuterated solvents, as indicated. TMS (0 ppm) was employed as standard. The elemental analysis (CHN) for the complexes was performed with a Perkin Elmer 2400 CHN analyzer. Infrared spectra were recorded with a Shimadzu FT-IR 8300 spectrophotometer. The solid sample was prepared in a KBr pellet and spectra were recorded over the frequency range of 400–4000 cm^{-1}. UV–Vis spectra for all the ligands and copper complexes were recorded in methanol with a UV–Vis Varian, Cary 50 Bio. Full scan mass spectra (MS mode) were obtained with a MicroTOF LC Bruker Daltonics spectrometer equipped with an electrospray source operating in positive ion mode. Samples were dissolved in a MeOH/H_2O (50/50) solution and were injected in the apparatus by direct infusion. The determination of melting points was made in the Microquimica MQAPF-301 apparatus. The electrical conductivity of solution of each complex (1×10^{-3} mol L^{-1}), in DMF, was measured with a Biocristal conductometer.

2.2. Synthesis

2.2.1. Synthesis of the ligands

The ligands N-(2-hydroxybenzyl)-N-(2-pyridylmethyl)amine (HL1), N-(2-hydroxybenzyl)-N-(2-pyridylmethyl)[(3-chloro)(2-hydroxy)]-propylamine (H2L2), 1-[2-hydroxybenzyl(2-pyridylmethyl)amino]-3-(1-naphthyloxy)-2-propanol (H2L3) and 1-[2-hydroxybenzyl (2-pyridylmethyl)amino]-3-(2-naphthyloxy)-2-propanol (H2L4) were synthesized as described in the literature (HL1: [22], H2L2: [23], H2L3 and H2L4: [19]).

2.2.2. Synthesis of [Pt^{II}(HL1)Cl] (1), [Pt^{II}(HL2)Cl] (2) and [Pt^{II}(HL4)Cl] (4)

The cited compounds (Scheme 1) were prepared in reactions between the ligands (HL1, 1 mmol, 214 mg; H2L2, 1 mmol, 307 mg; H2L4, 1 mmol, 414 mg) and K_2[$PtCl_4$] (1 mmol, 415 mg), in ethanol, with constant stirring at room temperature for 2 days. Thereafter, 50 mL of water was added to the solution, which was stirred for another day. After allowing the solution to stand for a few days, a light yellow (complex (**1**)), a light grey (complex (**2**)) and a beige solid (complex (**4**)) were filtered off, washed with cold propan-2-ol and dried in a desiccator. Table 1 shows some data concerning the synthesis and characterization of complexes (**1**)–(**4**).

2.2.3. Synthesis of [Pt^{II}(HL3)Cl] (3)

Complex (**3**) (Scheme 1) was prepared in a reaction between the

Table 1
Yield, elemental analysis (C, H, N), conductivity data (in DMF) and melting point (M.P.) for compounds (**1**)–(**4**).

Complex	Composition	Yield (%)/mass(mg)	%C (Found/Calcd)	%H (Found/Calcd)	%N (Found/Calcd)	Λ_M (cm^2 Ω^{-1} mol^{-1})	M. P. (°C)
(**1**)	$C_{13}H_{15}ClN_2O_2Pt$	62/290	33.47/33.81	3.11/3.27	5.86/6.07	17	295
(**2**)	$C_{16}H_{21}Cl_2N_2O_3Pt$	32/180	35.98/35.83	3.48/3.38	5.03/5.22	12	265
(**3**)	$C_{26}H_{27}ClN_2O_4Pt$	23/150	46.89/47.17	4.05/4.11	3.97/4.23	18	245
(**4**)	$C_{26}H_{27}ClN_2O_4Pt$	44/290	47.13/47.17	3.98/4.11	4.10/4.23	20	190

ligand H_2L3 (1 mmol, 414 mg) and $K_2[PtCl_4]$ (1 mmol, 415 mg), in ethanol/water 1:1, with constant stirring at room temperature for 24 h. Thereafter, the solution was filtered, rendering a brown solid (small amount) and 50 mL of propan-2-ol was added to the filtrated. After allowing the solution to stand for 6 days light yellow crystals were collected, washed with cold propan-2-ol and dried in a desiccator. Table 1 shows data concerning the synthesis and characterization of complex (**3**).

2.3. X-ray crystallography

X-ray diffraction data was carried out with a Bruker D8-Venture diffractometer equipped with the detector Photon 100 CMOS using microfocus MoKα (λ = 0,71,073 Å) X-ray radiation at 150 K. The collect, reduce and integrate data were performed utilizing APEX3 software [24]. Absorption correction was performed by a numerical method implemented in SADABS [25]. The structure was solved by intrinsic phasing [26] and refined by full-matrix least squares on F^2 with SHELX package [27]. The positions of hydrogen atoms were generated geometrically and refined according to a riding model. All non-hydrogen atoms were refined anisotropically. Selected crystallographic data are summarized in Table 2.

2.4. DFT calculations

Density functional theory calculations were performed in Gaussian 09 [28]. The B3LYP functional was used in conjunction with a mixed basis set consisting of LANL2DZ on platinum and 6-31G(d) on other atoms [29–33]. Solvation in water was modelled with the SMD implicit solvent model [34]. The least squares fit for (**3**) comparing the calculated and observed X-ray structures were performed using Mercury 3.8. and are shown in Fig. 2 [35]. A conformation search for complexes (**3**) and (**4**) was undertaken with Avogrado (V 1.2.0) using the UFF forcefield [36,37]. The Cartesian coordinates for the optimized geometries are listed in the Supplementary material, together with the following energies (in Hartree): B3LYP solution-phase electronic energy (E), and B3LYP solution-phase Gibbs free energy at 298.15 K and 1 M (G) and the results of the conformational search.

Table 2
Crystal data and structure refinement for (**3**).

Empirical formula	$C_{26}H_{25}ClN_2O_3Pt$
Formula weight	644.02
Temperature/K	150.0
Crystal system	Orthorhombic
Space group	$P2_12_12_1$
a/Å	10.5397(19)
b/Å	12.745(2)
c/Å	16.770(3)
α/°	90
β/°	90
γ/°	90
Volume/Å^3	2252.8(7)
Z	4
ρ_{calc}g/cm^3	1.899
μ/mm^{-1}	6.380
F(000)	1256.0
Crystal size/mm^3	0.316 × 0.105 × 0.094
Radiation	MoKα (λ = 0.71073)
2Θ range for data collection/°	4.014 to 51.374
Index ranges	$-12 \le h \le 12$, $-15 \le k \le 15$, $-20 \le l \le 20$
Reflections collected	35,933
Independent reflections	4288 [R_{int} = 0.0480, R_{sigma} = 0.0291]
Data/restraints/parameters	4288/0/299
Goodness-of-fit on F^2	1.111
Final R indexes [I ≥2σ (I)]	R_1 = 0.0198, wR_2 = 0.0389
Final R indexes [all data]	R_1 = 0.0237, wR_2 = 0.0405
Largest diff. peak/hole/e Å^{-3}	1.52/−0.63
Flack parameter	−0.009(4)

2.5. Antitumor activity

2.5.1. Culture of cells

Human leukemia cell lines THP-1 (acute monocytic leukemia cell line) and U937 (histiocytic lymphoma cell line), Molt-4 (acute lymphoblastic), Colo205 (human colon adenocarcinoma) and H460 (lung carcinoma) were cultured routinely in DMEM-F12 medium (Dulbecco's Modified Eagle Medium) (Gibco, BRL) supplemented with 10% fetal calf serum and gentamicin (20 μg·mL^{-1}, Gibco, BRL) at 37 °C in a humidified atmosphere containing 5% CO_2 in air. Culture media were changed every 2–3 days. Blood samples were collected from healthy donors in Sodium Heparin glass tubes "VacutainerTM" (Becton Dikinson) and the PBMC (peripheral blood mononuclear cells) isolated over Ficoll-Paque™ Plus (1.08 g·mL^{-1}) in a 50 mL conical tube (2:1 - blood:ficoll). Twenty milliliters of fresh heparinized blood sample were diluted in phosphate buffer saline (PBS), gently laid over 10 mL of Ficoll and centrifugated at 500 ×*g* for 20 min at 25 °C. PBMC were collected from the interface of spun blood samples and were washed three times with PBS by centrifugation at 500 ×*g* for 10 min at 4 °C. The supernatant was discarded and the cells were suspended in DMEM-F12 medium (Gibco, BRL). Trypan blue solution 0.4% (Sigma, Germany) was used to count the cells into an appropriate concentration and the viability of cells was checked; the required range of cells' viability is 95–99%.

2.5.2. Cell viability studies using the colorimetric MTT assay

The viability of the cells lines incubated with the platinum(II) complexes was evaluated by a MTT assay, as described by Mosman [38]. Tumoral and normal cells (THP-1, U937, Molt-4, Colo205, H460 and PBMC, respectively) were plated in 96-well plates at densities of 1×10^6 cells·mL^{-1}, and different concentrations of the Pt(II) coordination complexes (100, 50, 25, 12.5 and 6.5 μM) were added to the culture and maintained for 36 h at 37 °C. Previously, stock solutions of the platinum(II) complexes and ligands were prepared in DMSO (dimethyl sulfoxide) (2×10^{-2} M). Stock solutions of metallic salt and cisplatin were prepared in deionized water. In order to reach the desired concentrations, the stock solutions were diluted in DMEM-F12 medium (Gibco, BRL). Twenty microliters of 3-(4,5-dimethyl- 2-thihazyl)-2,5-diphenyl-2H-tetrazolium bromide (MTT) stock solution (5 mg mL^{-1}) were added into each well, containing 100 μL of complex, and the cells were incubated at 37 °C for 4 h. The formazan crystals were dissolved in acidic isopropanol and their absorbance was determined at 570 nm using a microplate reader (Thermo Labsystems Multiskan, 352 model). Each concentration was tested in three independent experiments run in triplicate. IC_{50} values were obtained from dose-response curves using GraphPad Prism 5.0 for Windows. Cisplatin (Sigma) was used as a positive control.

2.5.3. Measurement of Annexin V and propidium iodide staining

U937 were cultured at 1×10^6 cells mL^{-1} in 24 multiwell plates and treated with 22 μM of complex (**3**) for 24 h. Apoptosis was detected by using Annexin V-FITC Apoptosis Detection Kit. Briefly, after incubation, cells were washed twice with phosphate buffered saline (PBS) and incubated in 500 μL of binding buffer (100 mM HEPES/NaOH, pH 7.5, 1.4 M NaCl and 25 mM $CaCl_2$). To each sample, 5 μL of Annexin V-FITC and 10 μL of PI were added. Samples were incubated at room temperature for 10 min protected from light. Cell fluorescence was determined immediately with a flow cytometer (FACS Calibur-BD Sciences). The result was determined by recording 10,000 events per sample.

2.5.4. Study of cell cycle arrest by flow cytometric analysis

Cells were plated at 1×10^6 cells mL^{-1} in 24 multiwell plates and treated with complex (**3**) (22 μM) for 24 h in DMEM-F12 medium (Gibco, BRL). The incubated cells were then fixed in 70% ethanol at 4 °C for 30 min. Cells were stained with propidium iodide (PI) for 2 h in

darkness. The DNA content was measured by flow cytometer (FACS Calibur-BD Sciences) and cell cycle distribution was analyzed by WinMDI version 2.9 software. The proportions of cells in G_0/G_1, S, and G_2/M phases were represented as DNA histograms. Apoptotic cells with hypodiploid DNA content were measured by quantifying the sub-G_1 peak in the cell cycle pattern. The result was determined by recording 10,000 events per sample.

2.5.5. Analysis of mitochondrial membrane potential (ΔΨm) by flow cytometry using JC-1 stain

U937 cells were seeded at 1×10^6 cells mL^{-1} in 24-well plate and treated with complex (**3**) (22 μM) for 24 h in DMEM-F12 medium (Gibco, BRL). After the elapsed time, the cell suspension was transferred to a sterile tube and pelleted (400 ×*g*, for 7 min, at room temperature). Cells were stained with JC-1 dye (25 μg mL^{-1}) and incubate at 37 °C in a 5% CO_2 incubator for 15 min. The cells were washed twice with fresh medium and analyzed immediately by flow cytometry. JC-1 (5,5′,6,6′-tetrachloro-1,1′,3,3′ tetraethylbenzimidazolylcarbocyanine iodide) exists as a monomer in the cytosol (green) and also accumulates as aggregates in the mitochondria which stain red. In contrast, in apoptotic and necrotic cells, JC-1 exists in monomeric form and stains the cytosol green. Mitochondria containing red JC-1 aggregates in healthy cells are detectable in FL2 channel and express intact mitochondrial membrane potential (ΔΨm), whereas green JC-1 monomers in apoptotic cells are detectable in FITC channel (FL1) and express loss of (ΔΨm). The Mitochondria transmembrane potential (ΔΨm) was measured by flow cytometer (FACS Calibur) and was analyzed by WinMDI version 2.9 software.

2.5.6. Transmission electron microscopy (TEM) and scanning electron microscopy (SEM)

For TEM analysis, U937 cells were incubated with complex (**3**) at a concentration of 11 μM and after 4, 8 and 12 h of incubation the cell suspension was centrifuged at 100 ×*g* for 10 min, washed three times with phosphate-buffered saline (PBS; pH 7.2) and fixed by 2 h in 2.5% Glutaraldehyde, in 0.1 M sodium cacodylate buffer, post-fixed for 20 min in 1:1 solution osmium tetroxide (1%) and potassium ferricyanide (0.8%). For transmission electron microscopy, cells were dehydrated sequentially in a graded series of acetone (50–100%), and embedded in Epoxy resin (Poly/Bed® 812). Resin-embedded cells were placed in a silicon mold form well at 60 °C for 48 h for polymerization. The obtained blocks were sectioned and ultrathin sections (70 nm thick) were taken using an ultra microtome Reichert Ultracut S, collected on copper grids (400 mesh), stained with uranyl acetate and lead citrate, and observed in a Transmission Electron Microscope, TEM-900 (Zeiss, Germany). For SEM analysis, the cells were incubated with platinum complex in the concentration of 11 μM for 8 and 12 h. Fixed cells were dropped onto poly-L-lysine (Sigma®) precoated coverslips, post-fixed for 30 min. in 1:1 solution osmium tetroxide (1%) and potassium ferricyanide (0.8%), dehydrated sequentially in a graded series of alcohol (50–100%), and critical-point dried (Bal-Tec CPD 030 Critical Point Dryer) with CO_2. The samples were mounted on a stub of metal with adhesive, coated with 40–60 nm of metal such as Gold/Palladium (Sputter Coater SDC 050) and viewed in a Scanning Electron Microscope (JSM 6610 LV).

2.5.7. Determination of caspase activities

Caspases 3, 6, 8 and 9 activities were determined using the substrates VDVAD-pNA or DEVD-pNA (caspase 3 substrate), VEID-pNA (caspase 6 substrate), IETD-pNA (caspase 8 substrate), and LEHD-pNA (caspase 9 substrate) following the protocols of the Caspase Activity Assay kit from Invitrogen™ (ApoTarget™ caspase colorimetric protease assay kit). U937 cells (3-5 × 10^6 mL^{-1}) were incubated with 22 μM of complex (**3**) for 3 h and centrifuged at 400 ×*g* for 10 min. The supernatant was removed, and the pellet was suspended in 0.1 mL of lysis buffer and incubated on ice for 10 min followed by centrifugation at 10.000 ×*g* for 1 min. Protein concentrations were determined and cytosol extracts were diluted to a concentration of 50–200 μg protein per 50 μL cell lysis buffer (1–4 mg·mL^{-1}). Aliquots (50 μL) of the supernatant were removed and placed in a 96-well microplate containing reaction buffer (Invitrogen™). 5 μL of each substrate was added, and the microplate was incubated at 37 °C for 12 h. Activity was monitored as the cleavage and release of free pNA and quantified at 450 nm using a Microplate spectrophotometer (Epoch™, BioTek® Instruments, Inc.). Caspase activation of treated cells was compared with an uninduced control sample for the determination of the increase in caspase activity.

3. Results and discussion

3.1. Syntheses and structure of platinum(II) coordination compounds

The ligands H2L3 and H2L4 were designed to increase the antitumor activity of coordination compounds by adding naphthyl groups to the structure of the ligand HL1. This strategy proved to be successful previously where an increase in the antitumor activities for the analogous copper(II) and cobalt(III) complexes were reported [19,20]. As platinum(II) is an ion related to cisplatin, we decided to synthesize new platinum(II) compounds, containing the ligands HL1-H2L4, in order to investigated the effect of the naphthyl groups on the antitumoral activity of these compounds. The reactions between the ligands HL1-H2L4 and the platinum(II) salt $K_2[PtCl_4]$ resulted in pale colored compounds with average yield of 35%. The interaction between the ligand H2L3 and the Pt(II) salt appeared to be the most efficient. Table 1 shows that all the complexes were obtained in high purity and the conductivity suggested that they are neutral species. All four complexes are stable in air and soluble in polar solvents such as DMF, DMSO and slightly soluble in CH_3CN, ethanol, MeOH and chloroform.

3.2. Description of crystal structure of complex (3)

The compound (**3**) crystallizes in a non-centrosymmetric space group with one mononuclear platinum(II) complex per asymmetric unit. The Flack parameter was refined [−0.009(4)] indicating the occurrence of enantiopure crystal [39]. A perspective view of the molecule is displayed in Fig. 1. The relevant bond lengths and angles for complex (**3**) are listed in Table 3. In complex (**3**) the platinum(II) centre is coordinated by a σ-N_2OCl donor set provide by the ligand H2L3 *via* one amine nitrogen atom (N2), one pyridine nitrogen atom (N1), one phenolic oxygen atom (O1) and one chloro ligand (Cl1), resulting in a tetracoordinated platinum(II) complex. The geometry for Pt(II) complex is described as distorted square-planar. The presence of the deprotonated phenol group (O1) coordinated to the Pt(II) centre indicates greater Lewis acidity of the Pt(II) centre in complex (**3**) when compared with the previously reported copper(II) complexes containing the same ligand, in which the phenol group is protonated [19]. Similarly, in the Co(II) complex previously reported, containing the same ligand, the phenolic oxygen is deprotonated [20]. The H2L3-metal bond lenghts are slightly longer in the platinum compound than in cobalt and copper complexes, as an effect of the ionic radius presented by the metal ions.

3.3. DFT study

While the X-ray structure for (**3**) is known the structures of the other three complexes were not available. In order to gain further understanding of the probable structures of (**1**), (**2**) and (**4**) DFT calculations were employed using the known X-ray structural parameters for (**3**). An implicit solvent (water) model was included in order to mimic the medium employed in the biological studies. An initial trial showed that the methodology was able to reproduce the structural parameters around the square planar platinum(II) centre (Fig. 2) and orientation of the side-chain in (**3**); structural overlays (least squares fits) for this complex comparing the experimental (solid-state) and simulated (in

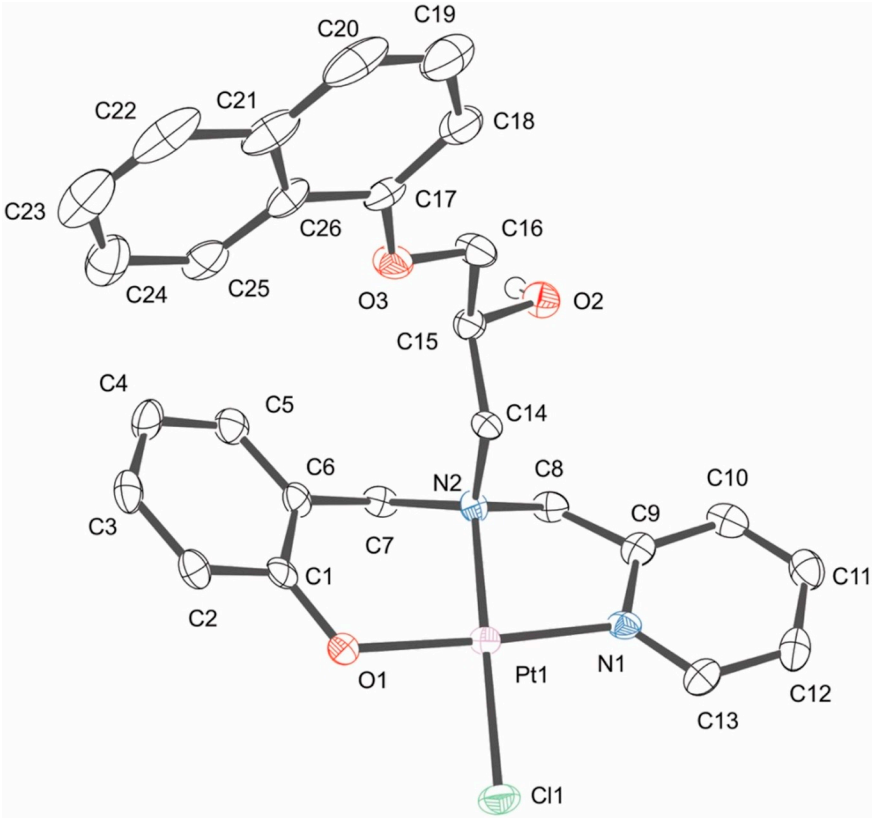

Fig. 1. View of the ORTEP-3 projections for complex (**3**) and the corresponding atom labeling scheme. Ellipsoids are shown at the 40% probability level.

Table 3
Selected bond and lengths (Å) and angles (°) for complex (**3**).

Pt1	Cl1		2.2909(15)
Pt1	O1		2.007(4)
Pt1	N2		2.055(5)
Pt1	N1		2.002(5)
O1	Pt1	Cl1	85.69(12)
O1	Pt1	N2	95.13(17)
N2	Pt1	Cl1	177.47(14)
N1	Pt1	Cl1	96.27(13)
N1	Pt1	O1	176.58(17)
N1	Pt1	N2	83.03(18)

water) structures are shown in Fig. 2. Based on the ability of the calculations to reproduce the structure of (**3**), the structures of complexes (**1**), (**2**) and (**4**) were calculated, again assuming the implicit solvent (water) model. For each of the complexes (**1**), (**2**) and (**4**) the known structure of (**3**) was modified using Avogadro [36] to accommodate the different side chains and the resulting Cartesian coordinates employed as input for the DFT calculations. The resulting structures are shown in Fig. 2. These calculations are not expected to represent the only possible structure of complexes (**1**), (**2**) and (**4**) in the biological medium. While the metal centre and tridentate ligand would be relatively rigid, the side chain is expected to have many possible conformations. The decision to focus only on a single conformation in the DFT study was made in order to examine how closely the DFT calculations were able to reproduce the structure of the complex in the region of the platinum centre. For complex (**3**), where the X-ray structure is available, the direct comparison shows that the calculations do show a close agreement between the X-ray crystal and DFT calculated structures. Therefore, the calculations are expected to reliably characterize the ML_4 centre of the other complexes. In terms of the enhanced antitumoral activity exhibited by complexes (**3**) and (**4**), the orientations of the α and β naphthyl groups are clearly of most interest. Several orientations of these naphthyl groups are possible and in order to probe this further, conformational studies were undertaken with complexes (**3**) and (**4**). For each complex a UFF conformer search revealed 26 low energy conformers [36,37]. The five or six lowest energy conformers are given in the Supplementary material. For (**3**) the spread of energies calculated for the five lowest energy conformers was 2.6 kcal/mol; all five of these would therefore be expected to be present at room temperature. One of these conformers corresponded to the conformer utilized in the DFT calculation (*i.e.* the one in the X-ray structure). For (**4**) the energy of the six most stable conformers differed by < 1.6 kcal/mol, the first five being practically identical in energy. The orientation of the naphthyl group in conformer 6 was equivalent to the structure utilized in the DFT calculation above. The calculations support the idea that the side chains of these complexes are flexible and multiple orientations of the α and β naphthyl groups are possible.

3.4. Infrared

Table 4 presents the characteristic IR bands of HL1-H2L4 ligands and their respective Pt(II) complexes. The IR spectra of complexes (**1**)–(**4**) were analyzed in comparison with those of their free ligands. For all the complexes, the main bands showed small shifts when compared to the respective free ligands (Table 4) The bands related to ν_{C-H} and $\nu_{C=N}$ exhibited downward (lower energy) after coordination to platinum(II) salt. The phenol group is deprotonated and it is coordinated to the platinum(II) centre as phenolate, as indicating by the absence of the bands at 1380, 1374, 1364 and at 1364 cm^{-1}, present in the ligands HL1-H2L4, respectively, attributed to δOH [20].

Based on the output from the DFT the calculated vibrational frequencies have been compared with the known infrared data for the four complexes. The resultant spectra are shown in the Supplementary material (Figs. S1–S4). The agreement between the calculated and

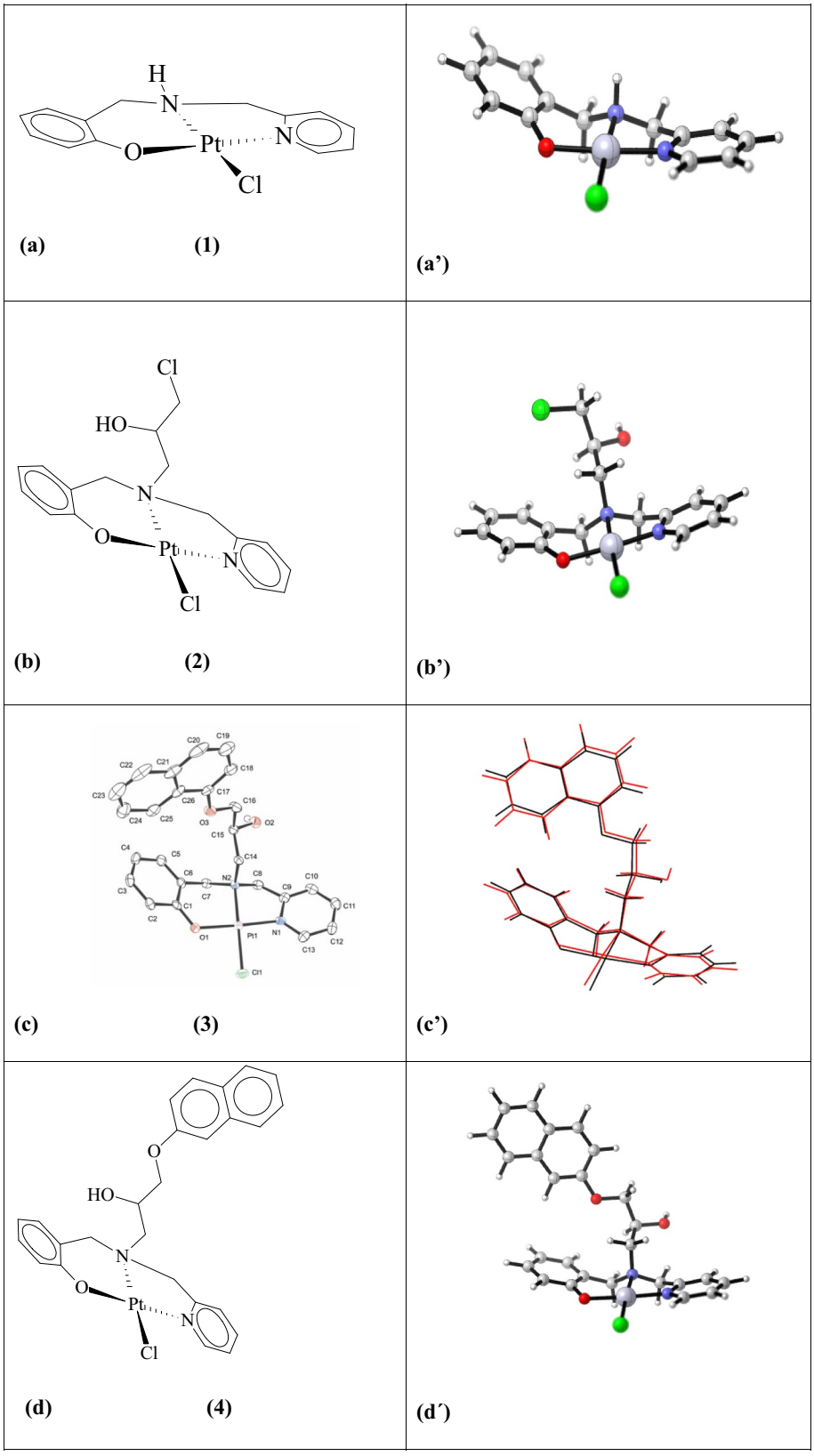

Fig. 2. Comparison of the proposed structures of (a) (**1**), (b) (**2**) and (d) (**4**) and (c) ORTEP picture of (**3**) with the calculated structures for (a′) (**1**), (b′) (**2**) and (d′) (**4**). For complex (**3**), an overlay of the calculated structure (black) with the X-ray (red) is presented in (c′).

Table 4
Characteristic IR bands (cm^{-1}) of the ligands HL1-H2L4 and their respective platinum(II) complexes.

Assignment	(1)	(2)	(3)	(4)
$\nu_{C-H\ aromatic}$	3088 (3032)	3088 (3053)	3069 (3053)	3073 (3053)
$\nu_{C=N}$	1595 (1595)	1599 (1581)	1598 (1569)	1599 (1569)
$\nu_{C=C}$	1450 (1438)	1452 (1458)	1445 (1449)	1448 (1449)
$\delta_{(pyridine\ ring)}$	767 (754)	769 (756)	762 (769)	758 (769)
$\delta_{(OH\text{-}phenol)}$	– (1380)	– (1374)	– (1364)	– (1364)

Data in parenthesis are related to the respective ligand.

experimental spectra is remarkably good, although further comparative structural information, other than the presence of the expected functional groups, would be speculative.

3.5. ESI(+)-MS and ESI(+)-MS/MS

ESI(+)-MS and ESI(+)-MS/MS of complexes (**1**)–(**4**) present a characteristic set of isopologue ions due mainly to the presence of metal and Cl atoms. For complex (**1**), the ESI(+)-MS data indicate the presence of peaks with *m/z* 426, 445, 516, 622, 659 and 851, revealing the presence of five mononuclear cations and one binuclear cation (*m/z* 851). The peaks with *m/z* 426, 445, 622, 659 and 851 are ascribed to the species $[Pt(II)(L1)(H_2O)]^+$, $[Pt(II)(HL1)(Cl)]^+$, $[Pt(II)(L1)(HL1)]^+$, $[Pt(II)(HL1)_2(Cl)]^+$ and $[(OH)Pt(II)(\mu\text{-}L1)_2Pt(II)(H_2O)]^+$. The peak with *m/z* 516 contains a fragmented ligand HL1 coordinated to the Pt (II) centre. For complex (**2**), the ESI(+)-MS data indicate the presence of peaks with *m/z* 501, 537, 549, 575 and 1037, revealing the presence of five mononuclear complexes and one binuclear complex in (*m/z* 1037). The peaks with *m/z* 501, 537, 549 and 575 are ascribed to the species $[Pt(II)(L2)]^+$, $[Pt(II)(HL2)(Cl)]^+$, $[Pt(II)(HL2)(H_2O)(formaldehyde)]^+$, $[Pt(II)(KL2)(Cl)]^+$ and $[(L2)Pt(II)(\mu\text{-}Cl)Pt(II)(L2)]^+$. These proposals are based on MS/MS data, which indicate that the species with *m/z* 1037 yields the cation with *m/z* 501, by the loss of a neutral molecule of 536 Da, described as a neutral complex [Pt(II)(L2)(Cl)]. For complex (**3**), the ESI(+)-MS data indicate the presence of peaks with *m/z* 542, 608, 1158 and 1251, revealing the presence of two mononuclear and two binuclear complexes (*m/z* 1251 and 1158). The peaks with *m/z* 608 and 1251are ascribed to the species $[Pt(II)(HL3)]^+$ and $[(HL3)Pt(II)(\mu\text{-}Cl)Pt(II)(HL3)]^+$. The peaks with *m/z* 542 and 1158 contain fragmented ligand coordinated to the Pt(II) centre. These proposals are based on MS/MS data, which indicate that the species with *m/z* 1251 yields the cation with *m/z* 1158, by the loss of a neutral molecule of 93 Da. The species with *m/z* 1251 also yields the cation with *m/z* 608 $[Pt(II)(HL3)]^+$, by the loss of a neutral molecule of 643 Da, ascribed as [Pt(II)(HL3)Cl]. For complex (**4**), the ESI(+)-MS data indicate the presence of peaks with *m/z* 415, 608, 916, 1022 and 1059, revealing the presence of four mononuclear species (*m/z* 608-1059). The peak with m/z 415 is ascribed to the protonated ligand $[H3L4]^+$. The peaks with *m/z* 608, 1022 and 1059 are ascribed to the species $[Pt(II)(HL4)]^+$, $[Pt(II)(H2L4)(HL4)]^+$ and $[Pt(II)(H2L4)(Cl)]^+$. The peak with *m/z* 916 contains fragmented ligand coordinated to the Pt(II) centre. These proposals are based on MS/MS data, which indicate that the species with *m/z* 1022 yields the cation with *m/z* 415, by the loss of a neutral molecule of 607 Da, ascribed as [Pt(II)(L4)]. Figs. S5–S8 shows the proposals for the main peaks presented in the ESI (+)-MS spectrum of complexes (**1**)–(**4**).

3.6. Assessment of cell viability by MTT assay

The cytotoxicity against cancer cell lines (Colo-205, H460, THP-1, U937 and Molt-4) were determined by means of the colorimetric MTT assay and the IC_{50} values were calculated in order to identify the more cytotoxic compounds and then to carry out studies related with the cell death mechanism. For a comparison of cytotoxicity, the compounds were also tested against peripheral blood mononuclear cells (PBMCs). Cisplatin, the prototype of many metal-based drugs, was also evaluated and included in some experiments as positive control for cell death. As presented in Table 5 the IC_{50} values were evaluated from the concentration dependence of viable cells 36 h after exposure to the platinum(II) compounds. As controls, we also tested the cytotoxic effects of the salt ($K_2[PtCl_4]$)and the ligands HL1-H2L4. Table 5 shows that, in general, complexes (**3**) and (**4**) are the most cytotoxic compound for all of the cell lines investigated, showing the effect of the presence of the naphythyl groups. Comparing the IC_{50} values for complex (**3**), (**4**) and their respective ligands (H2L3 and H2L4, respectively), complex (**3**) is slightly more cytotoxic than complex (**4**) against Colo-205, U937 and Molt- 4. It is worth noting that complex (**3**) is more active than complex (**4**) against the H460 cell line (IC_{50} = 51 ± 1 and 78 ± 1 μM, respectively) and THP-1 (6 ± 1 and 20 ± 1 μM, respectively). It is important to note that for the H460 cell line (lung cancer), cisplatin is not active, resulting in IC_{50} > 100 μM. Complexes (**3**) presents IC_{50} values lower than cisplatin toward Colo205 (30 and 41 μM, respectively), H460 (51 and > 100 μM, respectively), THP-1 (6 and 10 μM, respectively) and comparable to cisplatin toward U937 (11 and 8 μM, respectively) and Molt-4 (9 and 6 μM, respectively) cell lines. The greater cytotoxicity of complex (**3**) could be related to the ligand, since H2L3 is the most active ligand of this investigation, presenting IC_{50} values of 28 ± 1, 68 ± 1 and 43 ± 1 μM against U937, THP-1 and Molt-4 cells line, respectively. The low IC_{50} values indicate greater susceptibility of the leukemia cell lines U937, THP-1 and Molt-4 toward complexes (**3**) and (**4**) than to cell lines Colo-205 and H460, since leukemia cell lines are more sensitive than Colo-205 and H460. Similar results were obtained for cisplatin. Complexes (**3**) and (**4**), which contain naphthyl groups in their structures, presented IC_{50} values of 22 ± 1 and 42 ± 1 μM against PBMC. The value obtained for complex (**2**) is comparable to that determined for cisplatin (44 ± 1 μmol L^{-1}). Complexes (**3**) and (**4**), which contain naphthyl in their structures, presented IC_{50} values of 22 ± 1 and 42 ± 1 μM, respectively, against PBMC. Complex (**4**) exhibits a IC_{50} value comparable to cisplatin (44 ± 1 μM) against PBMC, suggesting that complex (**4**) is a promising complex, since presents lower IC_{50} value than cisplatin toward H460 (78 ± 1 and > 100 μM) and comparable IC_{50} values toward Colo-205, U937, THP-1, Molt-4 and PBMC.

Table 5
The 50% inhibitory concentration (IC_{50}) for the platinum complexes and their respective ligands, as well as $K_2[PtCl_4]$ and cisplatin, for leukemia (THP-1 U937 and Molt-4), colon (Colo-205), lung (H460) cancer cell lines and PBMC.

IC_{50} (μM)						
Compound	Colo-205	H460	U937	THP-1	Molt-4	PBMC
HL1	> 100	> 100	> 100[a]	> 100[a]	> 100[a]	–
H2L2	> 100	> 100	> 100	> 100	> 100	–
H2L3	> 100	> 100	28 ± 2	68 ± 2	43 ± 1	> 100
H2L4	> 100	> 100	> 100	> 100	> 100	> 100
$K_2[PtCl_4]$	> 100	> 100	> 100	> 100	> 100	–
(**1**)	> 100	> 100	72 ± 2	> 100	> 100	–
(**2**)	> 100	> 100	> 100	> 100	> 100	–
(**3**)	30 ± 2	51 ± 1	11 ± 1	6 ± 1	9 ± 1	22 ± 1
(**4**)	38 ± 2	78 ± 1	15 ± 2	20 ± 1	11 ± 2	42 ± 1
Cisplatin	41 ± 2	> 100	8 ± 1[a]	10 ± 1[a]	6 ± 1[a]	44 ± 2

[a] [40].

3.7. Mechanistic studies of cell death

Based on the cytotoxicity assessment presented in Table 5 complexes (**3**) and (**4**) were selected to investigate the mechanism by which they induce cell death in cancer cells. Therefore, we decided to investigate the mechanism by which complexes (**3**) and (**4**) induce cell death in the U937 cell line, in order to examine the effect of the

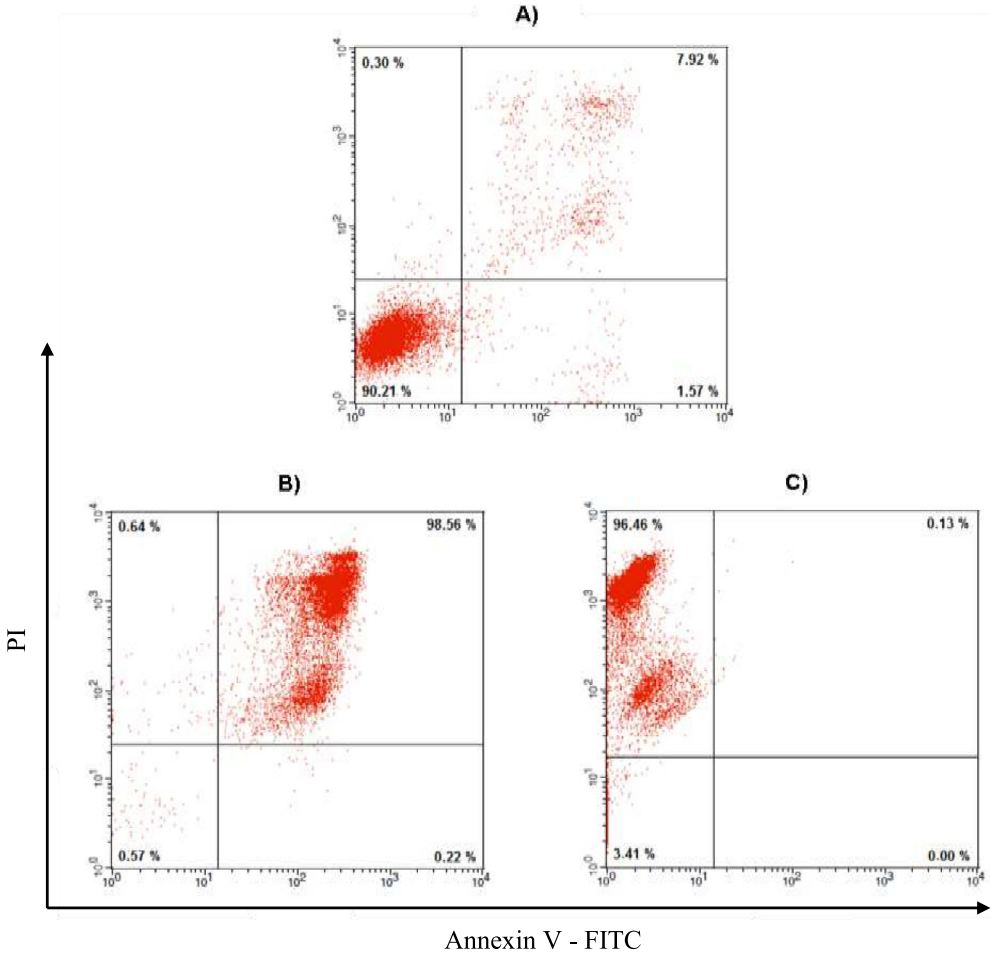

Fig. 3. Annexin V-FITC/PI staining detected apoptosis induced by complexes (**3**) and (**4**) in U937 cells, after treatment for 24 h. A) Control. B) U937 cells after treatment at the concentration of 22 μM of complex (**3**). C) U937 cells after treatment at the concentration of 30 μM complex (**4**). The data are presented in dot blots depicting Annexin V/FITC *versus* PI staining. The percentage of cells in each quadrant is presented.

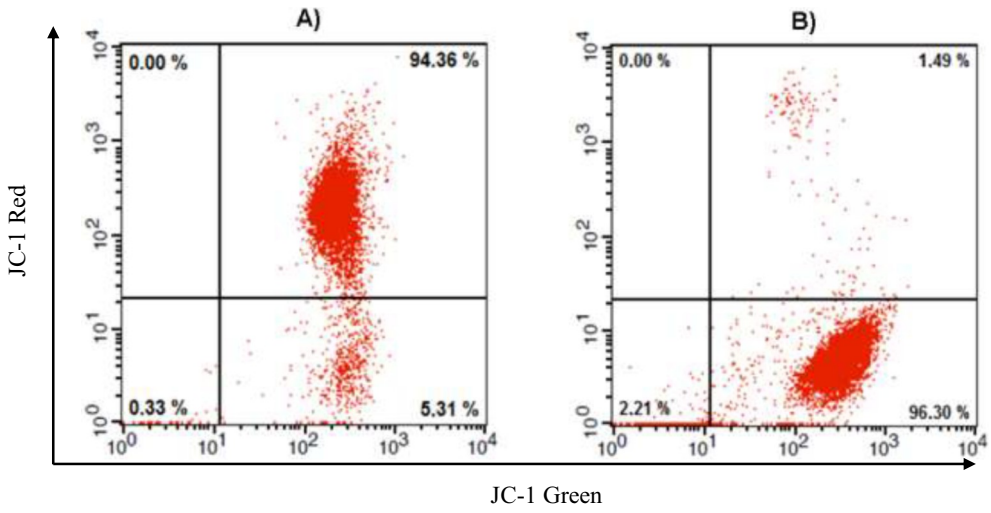

Fig. 4. Mitochondrial transmembrane potential (ΔΨm) assay. U937 cell line was incubated with 22 μM of complex (**3**) for 24 h. After being stained with JC-1, cells were analyzed by flow cytometry. Upper right quadrant - normal cells and lower right quadrant- loss of mitochondrial ΔΨm. A) Control cells. B) Cells after treatment with complex (**3**).

isomerism on the biological activity and compare these findings with those previously reported for Cu(II) and Co(II) complexes, containing the same ligands [19,20]. The first investigation was carried out by the measurement of apoptosis by Annexin V-FITC/PI analysis. Complex (**3**) showed high apoptosis rate (96%), the same value for cisplatin. However, complex (**4**) showed high necrosis rate (96%), after 24 h of treatment. Based on the results, the function of complex (**3**) in apoptosis was further investigated by analysis of mitochondrial membrane potential (ΔΨm), flow cytometric analysis of cell cycle arrest, transmission electron microscopy (TEM) and scanning electron microscopy (SEM).

3.7.1. Measurement of apoptosis by Annexin V-FITC/PI analysis

In order to confirm and quantify the extent of apoptosis, a double-

labeling technique using Annexin V-FITC and propidium iodide (PI) was utilized. In the flow cytometer dot plot cytogram analysis (Fig. 3) the lower left quadrant (negative for Annexin V and PI) is regarded as the population of live cells (normal), the one in the lower right quadrant (positive for Annexin V and negative for PI) illustrates the cell population at the early apoptosis stage, while the upper right quadrant (positive for Annexin V and PI) and the upper left quadrant (negative for Annexin V and positive for PI) represents the cell population at the late apoptosis stage and the necrotic cell population, respectively. Fig. 3 shows that after 24 h of treatment with 22 μM of complexes (**3**), 30 μM of complex (**4**) and the control. For the control (Fig. 3A), 90.21% of U937 are ascribed as normal cells and 7.92% were in upper right quadrant (late apoptotic stage). For the treatment with complex (**3**), (Fig. 3B) 98.56% were in upper right quadrant (late apoptotic stage) while for complex (**4**) (Fig. 3C) 96.46% were in the upper left quadrant, suggesting death by necrosis. As a positive control, U937 cells were incubated with 50 μM cisplatin and 29.8% of apoptotic cells were observed, suggesting that complex (**3**) was more effective than cisplatin (Fig. S9). So, based on these results, we decided to continue our investigation about the mechanism associated with the inhibition of U937 cell lines only promoted by complex (**3**), since this complex effectively induces apoptosis in these cells.

3.7.2. Analysis of mitochondrial membrane potential (ΔΨm)

As shown in Fig. 4, control cells of U937 show a strong red fluorescence (94.36%) after staining with JC-1. Following treatment of U937 cells with complex (**3**), for 24 h, the red fluorescence decreased to 1.49% (Fig. 4B). The lower right quadrant represents the cells with the loss of mitochondria ΔΨm indicating mitochondrial damage. The negative control and the treatment with complex (**3**) show 5.31 and 96.30% of cells in these quadrants, respectively. Positive control, treatment of U937 cell with cisplatin result in 88.04% of cell ΔΨm loss (Fig. S9). Our result shows that the treatment with complex (**3**) generates damage on mitochondria and suggests the involvement of intrinsic pathway of apoptosis.

These results are in good agreement with those obtained from MTT assay (Table 5) and indicate that the cytotoxicity of complex (**3**) against U937 cell line is mediated *via* apoptosis, which is directly related to mitochondrial dysfunction. The loss of mitochondrial potential is believed to occur through the formation of pores in the mitochondria.

3.7.3. Cell cycle analysis by flow cytometry

The relative cellular DNA content and distribution during the cell cycle was determined by flow cytometry (Fig. 5). In this study, U937 cells were incubated with complex (**3**) by 24 h and the results demonstrate the population of U937 cells in each phase of the cell cycle. The G1 phase, also called growth phase as it ensures that the cell is primed for DNA synthesis, plays a crucial role in cell cycle progression. As shown in Fig. 5, the population of U937 cells in the G1 phase changed from 44.64 in the control to 7.38% after treatment with complex (**3**). It is also worthwhile noting that the population of cells in the sub-G1, increased significantly upon the treatment with complex (**3**), resulting in change from 7.38 to 61.38%. Cisplatin positive control, U937 cell sub-G1 population increases from 0.26 to 89.52% after drug administration (Fig. S9). The increase of cell sub-G1 population corresponds to cell whose DNA has been cleaved by cellular nucleases that were activated by the apoptotic machinery. Thus, our results clearly show that complex (**3**) induces cell death by apoptosis. Furthermore, these results are in agreement with previous studies carried out with copper(II) and cobalt(II) complexes, obtained with the same ligand. These complexes promoted a decrease from 60% to 17% and from 60% to 20%, respectively, for copper(II) and cobalt(II) complexes, in the population of U937 cells in the G1 phase, after treatment with these complexes. The population of cells in the sub-G1, for treatment with these complexes increases significantly resulting in change from 0.2 (control) to 48% and from 7.73% to 83.56% after treatment with copper(II) and cobalt(II) complexes respectively.

3.7.4. Analysis of cell morphology by transmission electron microscopy (TEM) and scanning electron microscopy (SEM)

The cytotoxic effect of complex (**3**) (11 μM and time intervals of 4, 8 and 12 h) on the surface and the ultrastructural features on U937 cells was investigated by TEM and SEM. Representative images are presented in Figs. 6 and 7, respectively. U937 cells from the control group present a homogenous cytoplasm, with few and small regular mitochondrias (M). Some endoplasmic reticulum (ER) profiles as seen, indicating good cell status (Fig. 6A).

Transmission electron micrographs show that complex (**3**) causes changes in U937 cells by a time-dependent process, which presents apoptotic morphological patterns and initially targets the mitochondria. Fig. 6B shows the alterations after 4 h, Fig. 6C after 8 h and Fig. 6D after 12 h of treatment, respectively. As depicted in Fig. 6B, a significant increase in the number and size of the mitochondria is observed. Complex (**3**) induces alterations in the mitochondria, which present more rarefied mitochondrial matrix and changes in the arrangement of the mitochondrial ridges. After 8 h of treatment (Fig. 6C), the formation and releasing of elements like apoptotic bodies (A) can be clearly seen. Some of these apoptotic bodies present endoplasmic reticulum profiles and vacuoles. More elongated endoplasmic reticulum profiles (ER) and mitochondria (M) are seen in the cytoplasm. After 12 h of treatment

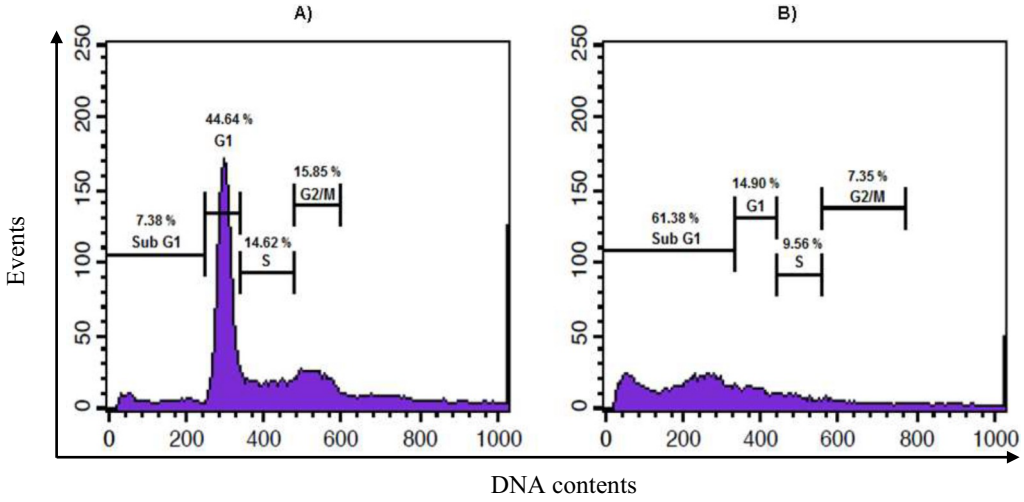

Fig. 5. Cell Cycle Analysis by Flow Cytometry. Leukemic cell line (U937) was stained with propidium iodide (PI) after 24 h of incubation without (control) and with complex (**3**). Cells with hypodiploid DNA content were measured by quantifying the sub-G1 peak in the cell cycle pattern. Each experiment per sample was determined recording 10.000 events. A) Control cells; B) cells after treatment with 22 μM of complex (**3**).

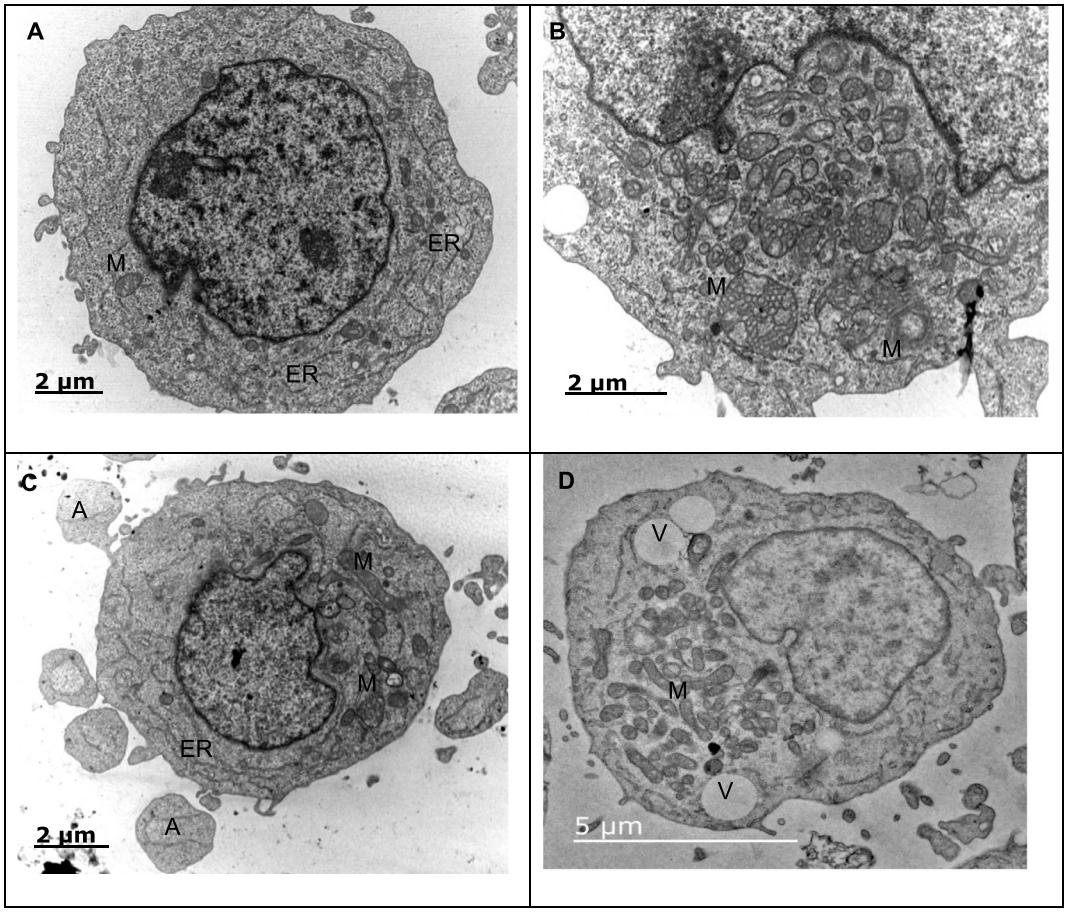

Fig. 6. Transmission Electron Microscopy of human leukemia cells. (A) Control cells, (B) U937 cell strain incubated with 11 µM of complex (**3**) for 4 h. Altered mitochondria [M] can be seen. (C) U937 cell line incubated for 8 h. Release of apoptotic bodies [A] can be seen at the cell periphery. Elongated endoplasmic reticulum [ER] and altered mitochondria [M] are also visible (D) U937 cell line incubated for 12 h, showing a great number of mitochondria [M] and cytoplasmic vacuoles [V].

with complex (**3**) (Fig. 6D), cytoplasm appears more rarefied. In some cells large vesicles and a diffuse cytoplasmic vacuolization have been observed, indicating that the cell is undergoing apoptosis, leading to inhibition of cell survival and proliferation demonstrating the cytotoxic effectiveness of complex (**3**) (Fig. 6D).

These data are in agreement with the loss of mitochondrial (ΔΨm) observed by JC-1 Mitochondrial Membrane Potential Sensor (Fig. 4) and may mean that the activity of complex (**3**) against leukemic cell lines is mediated by an apoptotic mechanism associated with mitochondrial dysfunction. Some platinum complexes, reported in the literature, induce damage in the mitochondria in a similar way to that promoted by complex (**3**), causing cell death by an intrinsic pathway [41,42].

Overall, our data suggest the triggering of the apoptotic signal, highlighting the differential effect of compound (**3**), which due to the structure of the ligand seems to act mainly on mitochondria. Similar results were observed by our research group for copper(II) and cobalt (II) coordination compounds, respectively [19,20].

By scanning electron microscopy, untreated U937 cells show preserved rounded form and the homogeneous presence of microvilli over all the cell surface, indicating a good viability (Fig. 7A). The results of the ultrastructural analysis by SEM shown significant changes in the cell surface with intense membrane blebbing after 8 h of treatment with complex (**3**) at concentration of 11 µM (Fig. 7B). Some cells appear to release apoptotic bodies [star] in the medium (Fig. 7C).

After 12 h of treatment, cells present reduction of surface blebbing, probably due to release of apoptotic bodies (Fig. 7D). Few microvilli are seen at the surface of treated cells after 12 h.

These data demonstrate that complex (**3**) had a significant cytotoxic effect, affected the cell morphology compared to the control, indicating ultrastructural changes characteristic of the apoptotic signal altering the dynamic properties of the plasma membrane.

The inhibitory activity of complex (**3**) appears to disrupt the proliferation and their invasiveness process of the U937 neoplastic cells. As a result of the treatment with complex (**3**) led to retraction of microvilli and phyllopodia, which is one way to inhibit metastasis, a feature considered fundamental to reduce the cancer malignancy [43,44].

Transmission electron microscopy (TEM) investigations are in agreement with the loss of mitochondrial potential (ΔΨm) and indicate that the activity of the complex (**3**) against leukemic cell line (U937) is mediated by an apoptotic mechanism associated with mitochondrial dysfunction (intrinsic pathway).

Fig. S10 shows transmission electron microscopy (TEM) investigations for cisplatin. Ultrastructural analysis of cisplatin-treated U937 cells showed cells with alterations in the nucleus (nuclear fragmentation and chromatin condensation). In addition, the integrity of the mitochondria seems quite compromised, some seem to be enlarged and emptied. The morphology of the mitochondrial ridges was altered when compared to the cells of the control group. The microvilli of the cell membrane also decreased considerably. In addition, few vacuoles were observed in the cytoplasm in relation to cells treated with the complex (**3**), where they were more notable.

Ultrastructural analysis of the surface of cisplatin-treated U937 cells is presented in Fig. S11. Cells with intense membrane blebbing within

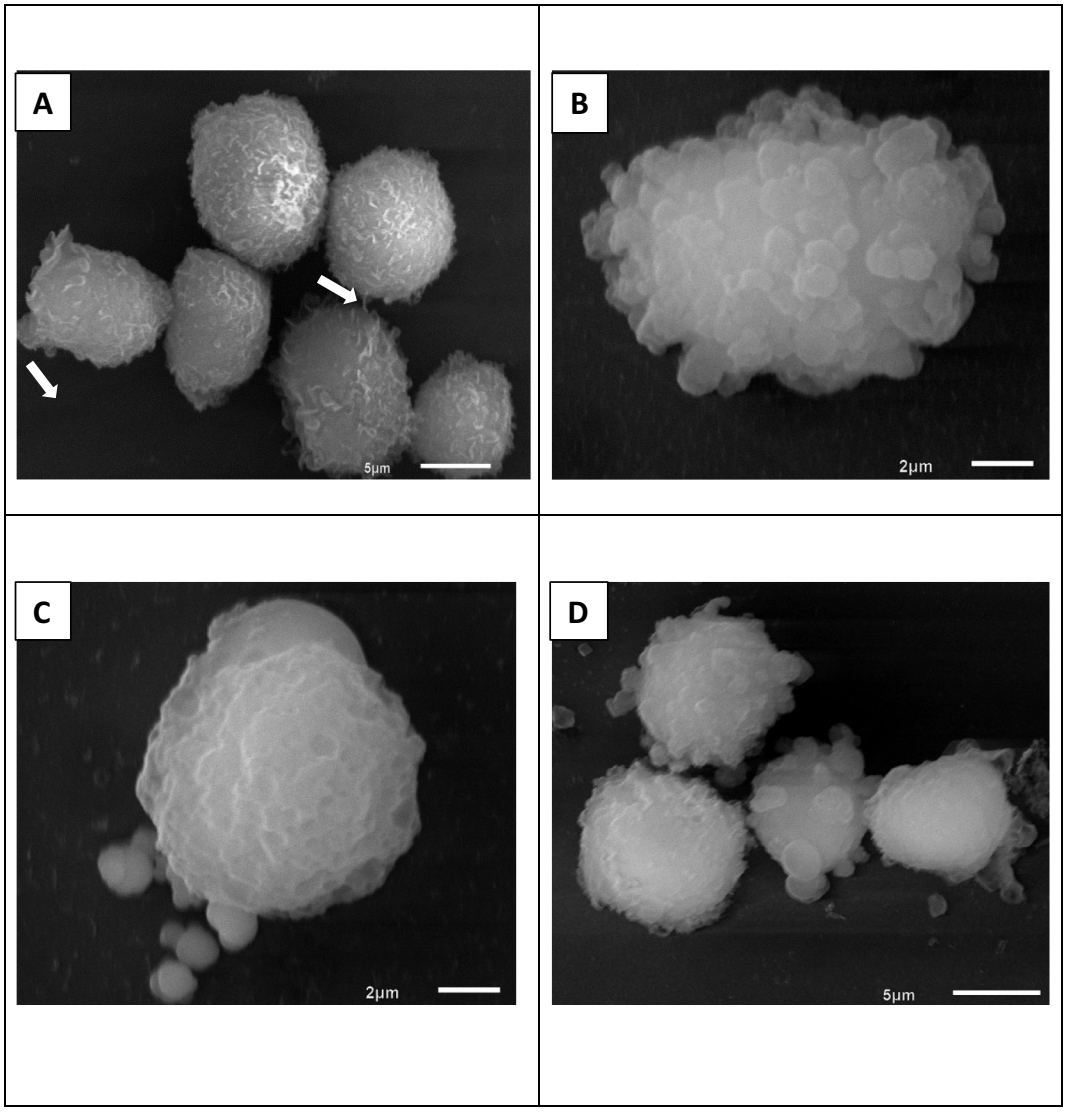

Fig. 7. Scanning Electron Microscopy of human leukemia cells (U937). (A) Control cells, showing microvilli [arrow] on the cell surface. (B) and (C) U937 cell line incubated with 11 μM of complex (**3**) for 8 h. The release of apoptotic bodies can be seen [star]. (D) U937 cell line incubated with 11 μM of the complex (**3**) for 12 h.

the first few hours of treatment are observed. In addition, the release of apoptotic bodies and the drastic reduction of cell membrane microvilli were detected mainly during the longer incubation times as the loss of its typical morphology when compared to the control group. These data emphasize the cytotoxic potential of cisplatin, and likewise demonstrate that complex (**3**) also affects the surface morphology of leukemic cells by inducing such changes, typical of the apoptotic process.

3.7.5. Determination of caspase activities

Considering that apoptosis may be triggered by extrinsic (*via* death receptor) and intrinsic (*via* mitochondrial) pathways, the activation of caspases 8, 9 (initiator caspases) and 3 and 6 (effector caspases) were analyzed (Fig. 8). After 3 h of incubation, all caspases were activated revealing high activity of complex (**3**) and suggesting that this complex may induce both apoptotic pathways (intrinsic and extrinsic). The activation of caspase 9 indicates that the apoptosis is related to damage in the mitochondria, showing agreement with TEM analyzes, which reveal alterations in the mitochondria after 4 h of incubation of U937 cells with complex (**3**).

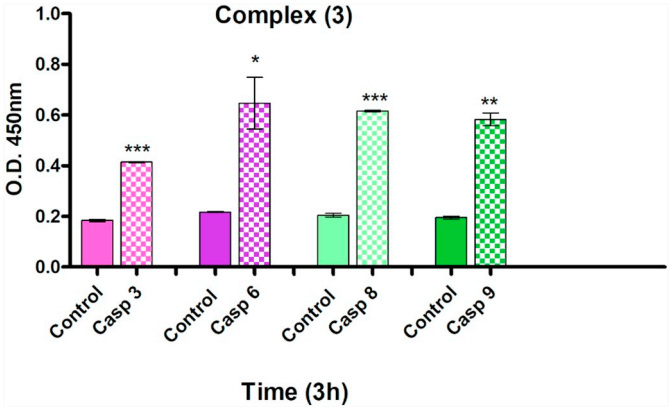

Fig. 8. Caspases 3, 6, 8 and 9 activation in U937 cells after treatment with complex (**3**). Cells were incubated with 22 μM of complex (**3**) for 3 h. Values are means ± S. D. from two separate measurements. *P < 0.05, **P < 0.01 and ***P < 0.001 *versus* control.

For the copper(II) complex obtained with the same ligand and reported previously by us [19], the apoptosis signal starts from a extrinsic pathway involving the activation of caspases 4 and 8, the signal is amplified by mitochondria with the concomitant release of cytochrome *c* and the activation of caspase 9. Then, the change of the metallic centre seems to modulate the pathway apoptotic, since the complex containing Pt(II) shows activation of caspases 3 and 9 after 3 h of incubation (intrinsic pathway, *via* mitochondrial) and the complex containing Cu(II) shows the activation of caspases 4 and 8 initially, after 6 h of incubation (extrinsic pathway, *via* death receptors). Activation assays of caspases 2, 3, 4, 8 and 9, after incubation of U937 cells with cisplatin, were previously published by us [19]. These results strongly suggest that cisplatin induces apoptosis in U937 cells mainly *via* the mitochondrial pathway.

Among the substrates cleaved by the caspases, there is a component of the cytoskeleton called actin, which, when cleaved, undergoes a rearrangement, alterations in cellular form and distribution of organelles. Then, cells undergo pyknotic and there is destabilization of the plasma membrane, generating protrusions called membrane blebbing, which are considered a specific pattern of apoptosis [44,45]. As shown in this work, such characteristics can be observed in SEM micrographs (Fig. 7) in response to the action of complex (**3**) on U937 cells.

4. Conclusions

In this study we have presented four new Pt(II) complexes. The naphthyl group is present in the structure of complexes (**3**) and (**4**) and is related to the higher antitumoral activity presented by these complexes. Complex (**3**) is slightly more cytotoxic than complex (**4**) against Colo-205, U937 and Molt- 4 and is the more active than complex (**4**) against H460 cell line (51 ± 1 and 78 ± 1 μM, respectively) and THP1- (6 ± 1 and 20 ± 1 μM, respectively). Complexes (**3**) presents IC_{50} values lower than cisplatin toward Colo205 (30 and 41 μM, respectively), H460 (51 and > 100 μM, respectively), THP-1 (6 and 10 μM, respectively) and comparable to cisplatin toward U937 (11 and 8 μM, respectively) and Molt-4 (9 and 6 μM, respectively) cell lines. X-ray diffraction studies was performed for complex (**3**) and DFT calculations indicate that, based on the known structure, all the calculated structures present the same coordination environment (N_2OCl) for the Pt centre. Then, based on DFT calculation, the better activities exhibited by complexes (**3**) and (**4**) are related to the presence of the α and β naphthyl groups, respectively.

The results presented herein show clearly the effect of isomerism on the mechanism of cell death, since complex (**3**) showed high apoptosis rate (98%) and complex (**4**) showed high necrosis rate (96%), after 24 h of treatment. Similar results were observed for complexes containing Cu (II) and Co(II) coordinated to the same ligands. This result indicates the modulation of the antitumoral activity by the insertion of the naphthyl groups, by the isomerism presented by the ligand and kind of metal center. Furthermore, the coordination of these known ligands to platinum(II) has resulted in new complexes with higher antitumoral activities than the copper and cobalt analogs. This study revealed that compound (**3**) promoted the activation of the initiator caspase 8 and 9 at the same time and, therefore, it is possible to conclude that it activates both intrinsic and extrinsic cell death pathways. This find differs from that observed for the copper compound, which initially activates only the extrinsic pathway.

Acknowledgements

The authors are grateful to financial support received from CAPES (Coordenação de Aperfeiçoamento de Pessoal de Nível Superior), CNPq (Conselho Nacional de Desenvolvimento Científico e Tecnológico)-472018/2012-4- and FAPERJ (Fundação de Amparo à Pesquisa do Estado do Rio de Janeiro)-E-26/111.360/2013. Computer resources were provided by the National Facility of the Australian National Computational Infrastructure and by the University of Queensland Research Computing Centre.

Appendix A. Supplementary data

Table S1, Relative energy for conformers for complexes (**1**)–(**4**), Cartesian coordinates for the optimized geometry for complexes (**1**)–(**4**) and Figs. S1–S9 in PDF format.

Crystallographic data (without structure factors) for the structure reported in this manuscript has been deposited with the Cambridge Crystallographic Data Centre as supplementary publication: deposition number: CCDC 1849033 for complex (**3**). Supplementary data to this article can be found online at https://doi.org/10.1016/j.jinorgbio.2018.12.016.

References

[1] D. Wang, S.J. Lippard, Nat. Rev. Drug Discov. 4 (2005) 307–320.
[2] T.C. Johnstone, G.Y. Park, S.J. Lippard, Anticancer Res. 34 (1) (2014) 471–476.
[3] K. Chválová, V. Brabec, J. Kaspárkiva, Nucleic Acids Res. 35 (6) (2007) 1812–1821.
[4] P. Heringova, J. Kasparkova, V. Brabec, J. Biol. Inorg. Chem. 14 (2009) 959–968.
[5] N.J. Wheate, S. Walker, G.E. Craig, R. Oun, Dalton Trans. 39 (2010) 8113–8127.
[6] L. Bai, C. Gao, Q. Liu, C. Yu, Z. Zhang, L. Cai, B. Yang, Y. Qian, J. Yang, X. Liao, Eur. J. Med. Chem. 140 (2017) 349–382.
[7] A.I. Matesanz, I. Leitão, P. Souza, J. Inorg. Biochem. 125 (2013) 26–31.
[8] A.A. Legin, S. Theiner, A. Schintlmeister, S. Reipert, P. Heffeter, M.A. Jakupec, J. Mayr, H.P. Varbanov, C.R. Kowol, M. Galanski, W. Berger, M. Wagner, B.K. Keppler, Chem. Sci. 7 (2016) 3052–3061.
[9] H. Chen, F. Chen, W. Hu, S. Gou, J. Inorg. Biochem. 180 (2018) 119–128.
[10] L.C. Batista, F.S. de Souza, V.M. de Assis, S.H. Seabra, A.J. Bortoluzzi, M.N. Rennó, A. Horn Jr., R.A. DaMatta, C. Fernandes, RSC Adv. 5 (2015) 100606–100617.
[11] L.J.H. Borges, E.S. Bull, C. Fernandes, A. Horn Jr., N.F.B. Azeredo, J.A.L.C. Resende, W.R. Freitas, E.C.Q. Carvalho, L.S. Lemos, H. Jerdy, M.M. Kanashiro, Eur. J. Med. Chem. 123 (2016) 128–140.
[12] N.F.B. Azeredo, F.P. Souza, F.C. Demidoff, C.D. Netto, J.A.L.C. Resende, R.W.A. Franco, P. Colepicolo, A.M.D.C. Ferreira, C. Fernandes, J. Mol. Struct. 1152 (2018) 11–20.
[13] C.A. Gomes, L.M. Lube, C. Fernandes, R.W.A. Franco, J.A.L.C. Resende, A. Horn Jr., New J. Chem. 41 (2017) 11498–11502.
[14] A. Horn Jr., A. Neves, I. Vencato, V. Drago, C. Zucco, R. Werner, W. Haase, J. Braz. Chem. Soc. 11 (1) (2000) 7–10.
[15] C. Fernandes, A. Horn Jr., O. Vieira-da-Motta, V.M. Assis, M.R. Rocha, L.S. Mathias, E.S. Bull, A.J. Bortoluzzi, E.V. Guimarães, J.C.A. Almeida, D.H. Russell, J. Inorg. Biochem. 104 (2010) 1214–1223.
[16] A. Horn Jr., L. Fim, A.J. Bortoluzzi, B. Szpoganicz, M.S. Silva, M.A. Novak, M.B. Neto, L.S. Eberlin, R.R. Catharino, M.N. Eberlin, C. Fernandes, J. Mol. Struct. 797 (2006) 154–164.
[17] A. Horn Jr., I. Vencato, A.J. Bortoluzzi, R. Hörner, R.A.N. Silva, B. Szpoganicz, V. Drago, H. Terenzi, M.C.B. Oliveira, R. Werner, W. Haase, A. Neves, Inorg. Chim. Acta 358 (2005) 339–351.
[18] A. Horn Jr., I. Vencato, A.J. Bortoluzzi, V. Drago, M.A. Novak, A. Neves, J. Braz. Chem. Soc. 17 (8) (2006) 1584–1593.
[19] C. Fernandes, A. Horn Jr., B.F. Lopes, E.S. Bull, N.F.B. Azeredo, M.M. Kanashiro, F.V. Borges, A.J. Bortoluzzi, B. Szpoganicz, A.B. Pires, R.W.A. Franco, J.C. de A. Almeida, L.L.F. Maciel, J.A.L.C. Resende, G. Schenk, J. Inorg. Biochem. 153 (2015) 68–87.
[20] S.R. Morcelli, E.S. Bull, W.S. Terra, R.O. Moreira, F.V. Borges, M.M. Kanashiro, A.J. Bortoluzzi, L.L.F. Maciel, J.C. de A. Almeida, A. Horn Jr., C. Fernandes, J. Inorg. Biochem. 161 (2016) 73–82.
[21] S.R. Morcelli, M.M. Kanashiro, D.R.S. Candela, M. Alzamora, A. Horn Jr., C. Fernandes, Inorg. Chem. Commun. 67 (2016) 22–24.
[22] A. Neves, M.A. de Brito, I. Vencato, V. Drago, K. Griesar, W. Haase, Y.P. Mascarenhas, Inorg. Chim. Acta 214 (1993) 5–8.
[23] A. Horn Jr., A. Neves, I. Vencato, V. Drago, C. Zucco, R. Werner, W. Haase, J. Braz. Chem. Soc. 11 (2007) 7–10.
[24] Bruker, APEX3 and SAINT, Bruker AXS Inc., Madison, Wisconsin, USA, 2015.
[25] L. Krause, R. Herbst-Irmer, G.M. Sheldrick, D. Stalke, J. Appl. Crystallogr. 48 (2015) 3–10.
[26] G.M. Sheldrick, Acta Cryst A71 (2015) 3–8.
[27] G.M. Sheldrick, Acta Cryst C71 (2015) 3–8.
[28] M.J. Frisch, G.W. Trucks, H.B. Schlegel, G.E. Scuseria, M.A. Robb, J.R. Cheeseman, G. Scalmani, V. Barone, B. Mennucci, G.A. Petersson, H. Nakatsuji, M. Caricato, X. Li, H.P. Hratchian, A.F. Izmaylov, J. Bloino, G. Zheng, J.L. Sonnenberg, M. Hada, M. Ehara, K. Toyota, R. Fukuda, J. Hasegawa, M. Ishida, T. Nakajima, Y. Honda, O. Kitao, H. Nakai, T. Vreven, J.A. Montgomery Jr., J.E. Peralta, F. Ogliaro, M. Bearpark, J.J. Heyd, E. Brothers, K.N. Kudin, V.N. Staroverov, T. Keith, R. Kobayashi, J. Normand, K. Raghavachari, A. Rendell, J.C. Burant, S.S. Iyengar, J. Tomasi, M. Cossi, N. Rega, J.M. Millam, M. Klene, J.E. Knox, J.B. Cross, V. Bakken, C. Adamo, J. Jaramillo, R. Gomperts, R.E. Stratmann, O. Yazyev, A.J. Austin, R. Cammi, C. Pomelli, J.W. Ochterski, R.L. Martin, K. Morokuma,

V.G. Zakrzewski, G.A. Voth, P. Salvador, J.J. Dannenberg, S. Dapprich, A.D. Daniels, O. Farkas, J.B. Foresman, J.V. Ortiz, J. Cioslowski, D.J. Fox, Gaussian 09, Revision D.01, Gaussian, Inc., Wallingford CT, 2013.
[29] A.D. Becke, J. Chem. Phys. 98 (1993) 5648–5652.
[30] C. Lee, W. Yang, R.G. Parr, Phys. Rev. B 37 (1988) 785–789.
[31] S.H. Vosko, L. Wilk, M. Nusair, Can. J. Phys. 58 (1980) 1200–1211.
[32] P.J. Stephens, F.J. Devlin, C.F. Chabalowski, M.J. Frisch, J. Phys. Chem. 98 (1994) 11623–11627.
[33] P.J. Stephens, F.J. Devlin, C.S. Ashvar, C.F. Chabalowski, M.J. Frisch, Discuss. Faraday Soc. 99 (1994) 103–119.
[34] A.V. Marenich, C.J. Cramer, D.G. Truhlar, J. Phys. Chem. B 113 (2009) 6378–6396.
[35] C.F. Macrae, I.J. Bruno, J.A. Chisholm, P.R. Edgington, P. McCabe, E. Pidcock, L. Rodriguez-Monge, R. Taylor, J. van de Streek, P.A. Wood, J. Appl. Crystallogr. 41 (2) (2008) 466–470.
[36] M.D. Hanwell, D.E. Curtis, D.C. Lonie, T. Vandermeersch, E. Zurek, G.R. Hutchison, J. Chemoinform. 4 (2012) 17.
[37] A.K. Rappe, C.J. Casewit, K.S. Colwell, W.A. Goddard III, W.M. Skiff, J. Am. Chem. Soc. 114 (25) (1992) 10024–10035.
[38] T. Mossmann, J. Immunol. Methods 65 (1983) 55–63.
[39] H.D. Flack, G. Bernardinelli, J. Appl. Crystallogr. 33 (2000) 1143–1148.
[40] C. Fernandes, A. Horn Jr., O. Vieira-da-Motta, M.M. Kanashiro, M.R. Rocha, R.O. Moreira, S.R. Morcelli, B.F. Lopes, L.S. Mathias, F.V. Borges, L.J.H. Borges, W.R. Freitas, L.C. Visentin, J.C. de A. Almeida, G. Schenk, Inorg. Chim. Acta 416 (2014) 35–48.
[41] S.M. Sancho-Martínez, L. Prieto-García, M. Prieto, J.M. López-Novoa, F.J. López-Hernández, Pharmacol. Ther. 136 (2012) 35–55.
[42] S. Dasari, Eur. J. Pharmacol. 740 (2014) 364–378.
[43] S.C. Grupta, J.H. Kim, S. Prasad, B.B. Aggarwal, Cancer Metastasis Rev. 29 (2010) 405–434.
[44] S. Al-Bahlani, B. Al-Dhahli, K. Al-Adawi, A. Al-Nabhani, M. Al-Kindi, Biomed. Res. Int. (2017) 1–13.
[45] M. Charpentier, S. Martin, Cancer 5 (2013) 1545–1565.